

4-2006

A spatially distributed model for the dynamic prediction of sediment erosion and transport in mountainous forested watersheds

Colleen O. Doten

Laura C. Bowling

Jordan S. Lanini

Edwin P. Maurer

Santa Clara University, emaurer@scu.edu

Dennis P. Lettenmaier

Follow this and additional works at: <https://scholarcommons.scu.edu/ceng>

 Part of the [Civil and Environmental Engineering Commons](#)

Recommended Citation

Doten, C.O., L.C. Bowling, J.S. Lanini, E.P. Maurer and D.P. Lettenmaier, 2006, A spatially distributed model for the dynamic prediction of sediment erosion and transport in mountainous forested watersheds, *Water Resour. Res.* Vol. 42, No. 4, W04417
doi:10.1029/2004WR003829.

Copyright © 2006 by the American Geophysical Union. AGU allows final articles to be placed in an institutional repository 6 months after publication.

This Article is brought to you for free and open access by the School of Engineering at Scholar Commons. It has been accepted for inclusion in Civil Engineering by an authorized administrator of Scholar Commons. For more information, please contact rsroggin@scu.edu.

A spatially distributed model for the dynamic prediction of sediment erosion and transport in mountainous forested watersheds

Colleen O. Doten,¹ Laura C. Bowling,² Jordan S. Lanini,¹ Edwin P. Maurer,³ and Dennis P. Lettenmaier¹

Received 19 November 2004; revised 21 July 2005; accepted 12 January 2006; published 25 April 2006.

[1] Erosion and sediment transport in a temperate forested watershed are predicted with a new sediment model that represents the main sources of sediment generation in forested environments (mass wasting, hillslope erosion, and road surface erosion) within the distributed hydrology-soil-vegetation model (DHSVM) environment. The model produces slope failures on the basis of a factor-of-safety analysis with the infinite slope model through use of stochastically generated soil and vegetation parameters. Failed material is routed downslope with a rule-based scheme that determines sediment delivery to streams. Sediment from hillslopes and road surfaces is also transported to the channel network. A simple channel routing scheme is implemented to predict basin sediment yield. We demonstrate through an initial application of this model to the Rainy Creek catchment, a tributary of the Wenatchee River, which drains the east slopes of the Cascade Mountains, that the model produces plausible sediment yield and ratios of landsliding and surface erosion when compared to published rates for similar catchments in the Pacific Northwest. A road removal scenario and a basin-wide fire scenario are both evaluated with the model.

Citation: Doten, C. O., L. C. Bowling, J. S. Lanini, E. P. Maurer, and D. P. Lettenmaier (2006), A spatially distributed model for the dynamic prediction of sediment erosion and transport in mountainous forested watersheds, *Water Resour. Res.*, 42, W04417, doi:10.1029/2004WR003829.

1. Introduction

[2] The effect of forest disturbance and management on aquatic resources in mountainous terrain is a problem of considerable contemporary scientific and public concern. The relationship between land use and erosion in mountainous forested watersheds has been known in a qualitative sense for some time. Vegetation management, forest road construction and forest fires impact basin sediment yield by increasing the amount of sediment available for transport and the amount of surface water available to transport it. Vegetation removal increases rates of surface erosion and mass wasting, temporarily until vegetation is reestablished or permanently depending on the type of vegetation that establishes. Forest roads affect basin hydrology and mass wasting through interception and redirection of subsurface flow, and they are another source of surface sediment in these environments.

[3] Various predictive models have been developed to assess the effects of forest management on sediment generation and transport. These models range from the empirically based universal soil loss equation (USLE) [*Wischmeier and*

Smith, 1965], developed to provide estimates of average annual sediment yield for agricultural applications, to models such as SHETRAN/SHESED [*Wicks and Bathurst*, 1996; *Burton and Bathurst*, 1998], built on the System Hydrologique European (SHE) hydrology model. SHETRAN/SHESED represents surface erosion, mass wasting (deterministically by predicting failure locations with mean soil and vegetation parameters), sediment delivery to channels and channel routing. Other model applications in forested watersheds include WEPP [*Ascough et al.*, 1997], dSLAM [*Wu and Sidle*, 1995], IDSSM [*Dhakal and Sidle*, 2003], and GEOTOP [*D'Odorico et al.*, 2005]. However, an approach that represents forest roads and their effects on basin hydrology and mass wasting, as well as erosion of road surfaces and routing of eroded sediment to and through the channel network has yet to be developed.

[4] The approach we describe here is intended to estimate sediment delivery and channel transport in mountainous, forested watersheds, and to address shortcomings in existing methods for prediction of effects of forest management and disturbance regimes on sediment generation. Our approach is based on the existing distributed hydrology-soil-vegetation model (DHSVM) hydrologic construct [*Wigmosta et al.*, 1994; *Wigmosta and Lettenmaier*, 1999]. DHSVM is a spatially distributed hydrological model that explicitly represents the effects of topographic and subsurface heterogeneities on the downslope redistribution of subsurface moisture. It was designed to provide a physically based tool to address the hydrologic consequences, especially changes in flood potential, associated with disturbances (logging, fire, forest roads) in forested mountainous watersheds. DHSVM

¹Department of Civil and Environmental Engineering, University of Washington, Seattle, Washington, USA.

²Department of Agronomy, Purdue University, West Lafayette, Indiana, USA.

³Department of Civil Engineering, Santa Clara University, Santa Clara, California, USA.

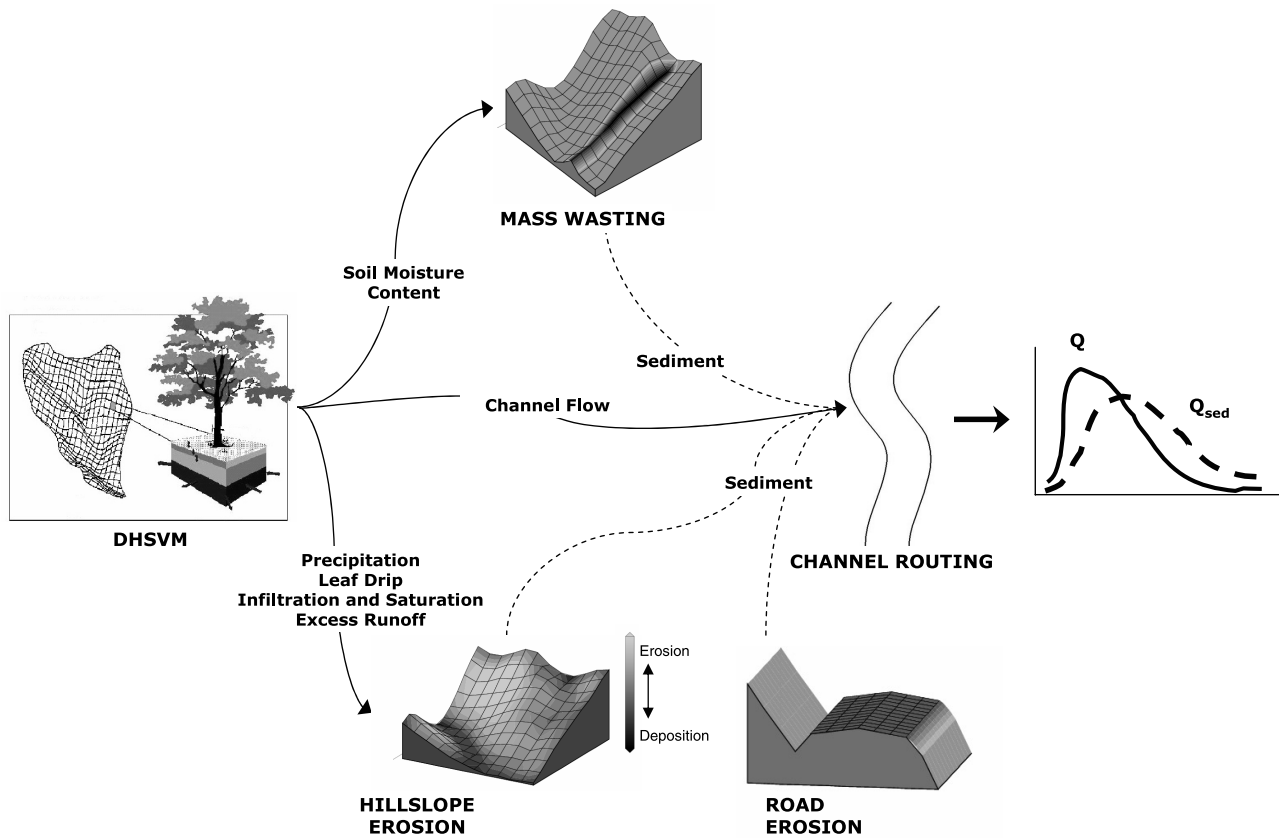


Figure 1. Sediment module schematic.

has been applied to a number of catchments in the western U.S. [Storck *et al.*, 1998; Leung and Wigmosta, 1999; Bowling and Lettenmaier, 2001; LaMarche and Lettenmaier, 2001] and Canada [Nijssen *et al.*, 1997; Wigmosta and Perkins, 2001; Whitaker *et al.*, 2002, 2003].

2. Model Description

[5] The sediment model consists of four primary components: mass wasting, which is stochastic in nature; hillslope erosion; erosion from forest roads; and a channel-routing algorithm. DHSVM provides a continuous temporal sequence, spatially distributed over a watershed, of the following variables used in the erosion and mass wasting computations: depth to fully saturated soil, saturation and infiltration excess runoff, precipitation, leaf drip, and channel flow (Figure 1).

[6] The sediment model follows the same conceptual foundation that has been used in stochastic slope-stability models [e.g., Hammond *et al.*, 1992; Koler, 1998]. The main difference is that slope failures are based on the dynamic simulation of soil saturation by DHSVM, from which time-varying pore pressure, and hence failure probabilities, are computed. The conceptual framework also draws from the SHETRAN/SHESSED modeling system which incorporates mass failures and rule-based redistribution of sediment [Wicks and Bathurst, 1996; Burton and Bathurst, 1998]. Major differences between our (DHSVM) sediment model and the SHETRAN/SHESSED modeling system are the use of stochastic mass failure predictions and the representation of forest roads.

In the remainder of this section we describe each of the four primary components.

2.1. Mass Wasting

[7] The mass-wasting algorithm has two primary functions: failure prediction and downslope redistribution of material released from slope failures. This component is stochastic in nature and results in an event probability of failure.

2.1.1. Failure Prediction

[8] Failure prediction is based on the concept that hydrological triggering of mass failures occurs when local pore pressure reduces shear strength below the imposed stresses (so-called factor of safety less than one). Soil saturation is determined within DHSVM using the subsurface routing scheme of Wigmosta and Lettenmaier [1999]. The mass wasting algorithm runs only for the single time step with the greatest basin saturation extent during an event (events can be identified by various means, but we use an approach similar to the peaks-over-threshold method used in flood frequency analysis). Our approach is similar in this respect to the approach used by Benda and Dunne [1997], who used the largest storm of the year to model landsliding and debris flows stochastically. An event is defined as a time period where saturation thresholds are met and is bracketed by two days, preceding and following, when those thresholds are not met.

[9] The mass wasting algorithm calculations are performed at a finer spatial resolution than used by DHSVM for its hydrological computations. Soil moisture at the DHSVM resolution is redistributed to the fine resolution

using the topographic index of *Beven and Kirkby* [1979]. The fine resolution soil moisture deficit (soil depth minus water table thickness) is related to the wetness index as [*Burton and Bathurst*, 1998]:

$$(z_i - \bar{z}) = \frac{\bar{I} - I_i}{f} \quad (1)$$

Where z_i is the soil moisture deficit for each fine resolution cell, i , \bar{z} is the average over all fine resolution grid cells (equal to the DHSVM resolution soil moisture deficit), I_i and \bar{I} are the grid cell and mean topographic wetness index, respectively, and f is a parameter governing the exponential decrease of hydraulic conductivity with depth. Following calculation of the individual z_i values, they are further screened to be between 0 and the local soil depth.

[10] Once the fine-resolution saturation deficit is determined, factor of safety computations begin and are performed on a grid cell by grid cell basis. Screening criteria are used throughout the algorithm to limit computations to critical areas. The first criterion ensures that the fine mesh grid cell is a potential sediment source (i.e., it was not removed during previous failures, in either the current or previous time steps), and the saturation is greater than a fixed threshold. Second, the slope in the direction of steepest descent, calculated based on the sediment elevation of eight neighboring grid cells, must be greater than 10° . This limit was conservatively selected because reported values and slope stability theory indicate that shallow landslides are infrequent on slopes less than 25° [*Sidle et al.*, 1985; *Reneau and Dietrich*, 1987; *Burton and Bathurst*, 1998]. If these criteria are not met, the grid cell cannot fail, and the model does not perform factor of safety computations.

[11] If the above criteria are met, factor of safety (FS) analysis is conducted based on the infinite slope model [e.g., *Ward et al.*, 1981; *Selby*, 1982; *Burton and Bathurst*, 1998]. Instability (grid cell failure) is indicated by FS values less than one. The algorithm generates stochastic results through the use of prescribed probability distributions (either normal, triangular, or uniform) for four of the parameters that define shear strength and loading: soil cohesion, angle of internal friction, root cohesion and vegetation surcharge (loading due to the mass of vegetation on the soil column). In our implementation, the probability distributions and their parameters are based on published values [see *Doten and Lettenmaier*, 2004]. In some instances the randomly selected parameters may result in unconditional (not a function of soil moisture) instability. We determined that these apparent instabilities were due either due to a combination of stochastic parameters that would not be physically realistic or due to inconsistent values for slope and soil depth, representing pixels that would likely have already failed and therefore would not have any material available for transport. For this reason, these pixels are not permitted to fail (soil is constrained to be immobile).

2.1.2. Mass Redistribution

[12] The rule-based redistribution of failed material involves estimation of the failure volume, as well as the direction and distance of movement. Instead of imposing a landslide size, failures occur one grid cell at a time; and therefore the minimum failure width is equal to the narrowest grid dimension. All the sediment on the failed grid cell is

routed downslope, in the direction of steepest descent based on the bedrock slope. The failure calculations then proceed in this downslope direction. The slope associated with the downslope cell is recalculated accounting for the changes in sediment depth, and the FS is calculated with the new slope and soil loading. If this grid cell fails, the failure continues to propagate downslope. At any time the failure encounters a channel, the material enters the channel network. If a channel is not encountered, the failure ceases to propagate when a stable pixel is reached. Then the material runs out until a slope less than a fixed threshold (which we have taken as four degrees following *Burton and Bathurst* [1998]), is encountered. The wasted material is evenly distributed along the runout path of unfailed cells following *Burton and Bathurst* [1998]. Material that enters the channel network can travel through the network as a debris flow.

[13] In DHSVM, the channel network is represented by a series of connected reaches (vectors) and each reach may span multiple grid cells. If the junction angle between reaches (measured as the angle between the two vectors pointed in the downstream direction) is less than 70° , movement continues as a debris torrent [*Benda and Dunne*, 1997]. For junction angles greater than 70° (i.e., the tributary enters at a more perpendicular angle), all transported sediment is divided equally between the upstream and downstream channel segments and downstream transport stops. Debris flows also stop and deposit all transported sediment if the channel segment slope (required input for DHSVM) falls below a fixed threshold, which we take as 3.5° following *Benda and Dunne* [1997]. Because failures are tracked downslope from the initial failed grid cell, if a failure has already occurred for a given pixel at the same time step (e.g., as a consequence of failure of an upslope cell) it is not allowed to fail again.

[14] This process is repeated for multiple ensemble members, and every time a FS is calculated, new parameters are selected from the specified distributions. Therefore the same grid cell will have different parameters for each event and each ensemble member in that event. The changes in sediment depth due to mass wasting and deposition are tracked for each ensemble member. After computations have been performed for all ensemble members for the current time step, the changes in sediment depth are averaged to create a sediment map. The amount of sediment added to each channel segment, from debris flow routing, is also averaged over the ensemble members. The averaged sediment map and channel segment sediment loads become the initial condition for the next model time step.

2.2. Surface Erosion

[15] The surface erosion algorithm represents the mechanisms by which sediment is eroded from hillslopes and forest roads and transported to the stream or roadside ditch network. It is deterministic in nature, and therefore is unconnected to the failure scenarios predicted by the mass wasting algorithm. Surface erosion is computed at the DHSVM spatial resolution, rather than the higher resolution of the mass wasting algorithm. We assume that there is unlimited sediment available for detachment.

[16] Runoff generation from each grid cell, including infiltration and saturation excess runoff, and culvert return flow is determined by DHSVM, as described by *Wigmosta et al.* [1994] and *Wigmosta and Perkins* [2001], with

corrected inconsistencies in the runoff routing direction including checks to account for depressions and flat areas in the digital elevation model (DEM). Infiltration excess runoff is based on either a static (previously used by DHSVM) or dynamic (*Smith and Parlange* [1978] in the manner of KINEROS [*Smith et al.*, 1995]) maximum infiltration capacity for surface erosion calculations.

[17] If a grid cell contains a road, for routing purposes runoff is partitioned between the road and hillslope based on the area of the road in the grid cell. For both surfaces, overland flow is modeled using an explicit finite difference solution of the kinematic wave approximation to the Saint-Venant equations [*Chow et al.*, 1988]. The solution time step is calculated dynamically according to the Courant condition to maintain solution stability while minimizing run time.

[18] The algorithm uses methods for surface erosion prediction similar to the mechanistic models EUROSEM [*Morgan et al.*, 1998], SHESED [*Wicks and Bathurst*, 1996] and KINEROS [*Woolhiser et al.*, 1990]. Sediment available for transport is routed using a four-point finite difference solution of the two-dimensional conservation of mass equation such that total erosion is limited by transport capacity [*Wicks and Bathurst*, 1996]:

$$\frac{\delta(QC)}{\delta x} + \frac{\delta(AC)}{\delta t} = e(x, t) \quad (2)$$

where Q is inflow of water (m^3/s); A is the cross-sectional area of flowing water (m^2); C is the current local sediment concentration (m^3 sediment/ m^3 water); x is horizontal distance (m); t is time (s); and e is the net erosion (m^2/s).

2.2.1. Hillslope Erosion

[19] Hillslope sediment supply is calculated based on detachment energy of raindrops, leaf drip, and overland flow. Raindrop detachment is calculated according to *Wicks and Bathurst* [1996] and is proportional to the fraction of vegetative cover (both understory and overstory), the momentum of throughfall and leaf drip, and an empirical soil erodibility coefficient. It also accounts for reduced detachment with increasing runoff depth.

[20] Water and sediment routing calculations proceed from the highest grid cell to the lowest. Overland flow is routed prior to implementation of the erosion algorithm, so the depth and velocity of flow are available for sediment calculations. Overland flow is calculated as uniform sheet flow over the entire pixel. Sediment transport is calculated using a modified version of the finite difference equations used by the SHETRAN/SHESED model [*Wicks and Bathurst*, 1996]:

$$C_i^t = \frac{\left\{ C_{i-1}^t \left[\frac{\theta}{\Delta x} Q_{i-1}^t - \frac{\alpha}{2\Delta t} Q_{i-1}^{\beta} \right] + C_{i-1}^{t-1} \left[\frac{\alpha}{2\Delta t} Q_i^{(t-1)\beta} - \frac{1-\theta}{\Delta x} Q_i^{t-1} \right] + C_{i-1}^{t-1} \left[\frac{\alpha}{2\Delta t} Q_{i-1}^{(t-1)\beta} + \frac{1-\theta}{\Delta x} Q_{i-1}^{t-1} \right] + D_r + D_{of} \right\}}{\left[\frac{\alpha}{2\Delta t} Q_i^{\beta} + \frac{\theta}{\Delta x} Q_i^t + \beta_{de} \Delta y v_s \right]} \quad (3)$$

where the Q is runoff, m^3/s , and Δx and Δy are the grid cell dimensions, m. The left side of this equation is the sediment outflow concentration from the cell, m^3/m^3 , for the current sub-time step; the first three terms on the right side are the inflow concentration from the upslope grid cell at the current sub-time step, and the outflow concentration from

the previous sub-time step from the current grid cell and upslope grid cell, respectively. Area was defined in terms of Q using Manning's equation, resulting in: $\alpha = n * \Delta x^{2/3}/S^{1/2}$ and $\beta = 2/3$. The time weighting factor, θ , is initially set to 0.55. The last two terms on the right side are D_r , soil detached by raindrop impact, $\text{m}^3/\text{s}/\text{m}$ and D_{of} , soil detachment from overland flow, $\text{m}^3/\text{s}/\text{m}$, which is equal to $\beta_{de} \Delta y v_s TC$, where β_{de} represents detachment efficiency, v_s is the settling velocity, m/s, and TC is the transport capacity, m^3 sediment/ m^3 water.

[21] Although the surface erosion calculations imply sheet flow, adjustment of the detachment efficiency effectively incorporates some processes such as rill erosion that are not specifically represented. Absent a physical representation, an empirical detachment efficiency parameter was used to represent the increased detachment from flow concentration in a similar manner to *Morgan et al.* [1998]. Particle detachment is known to be related to soil cohesion, among other things [*Morgan et al.*, 1998]. We determine β_{de} from soil cohesion, but in a slightly different manner:

$$\beta_{de} = 0.79e^{-0.6C_s} \quad (4)$$

where C_s is soil cohesion in kPa. Transport capacity is determined according to the unit stream power method of KINEROS [*Woolhiser et al.*, 1990]. This assumes that outflow is a power function of unit storage, as done by *Smith et al.* [1995], *Morgan et al.* [1998] and *Ziegler et al.* [2001]. In our application, the transport capacity of flow with depths less than 0.001 m is assumed to be zero since model tests based on maximum concentrations reported by *Govers* [1992] indicate this is a critical value.

[22] If the flow is unable to carry the calculated sediment outflow, deposition will occur. The mass of sediment outflow for the current sub-time step accumulates for each sub-time step (as determined by the Courant condition), up to the DHSVM time step.

2.2.2. Forest Road Erosion

[23] Road surface flow does not travel from cell to cell within DHSVM but rather enters the roadside ditch in the grid cell in which it was generated [*Wigmosta and Perkins*, 2001]. We retain this convention, although routing now accounts for road crown type. Water is routed across the road to the roadside ditch, and/or to the hillslope depending on whether the road is crowned, in-sloped or out-sloped.

[24] Forest road erosion is modeled similarly to the hillslope erosion and in the manner of KINEROS [*Woolhiser et al.*, 1990; *Ziegler et al.*, 2001]. Total erosion is calculated based on raindrop impact and overland flow detachment.

Soil particle detachment by raindrop impact is calculated based on the rainfall intensity and an empirical soil erodibility coefficient. It also accounts for reduced detachment with increasing runoff depth. Erosion is limited by transport capacity, which is calculated using the same method as for hillslope erosion except that the stream power threshold is

set at a lower threshold of 0.0004 m/s and for flow depths less than the median particle size (d_{50}), transport capacity is zero.

[25] Sediment is also routed according to the crown slope: i.e., if the road is in-sloped, sediment is added to the roadside ditch, or if the road is crowned half the sediment is routed to the hillslope and half to the roadside ditch. Sediment from the road surface and hillslope are available for transport through the roadside ditch network. All roadside ditch segments have culverts and all sediment that is routed to the culvert is discharged through the culvert. If the culvert is in a grid cell with a stream channel, a portion of the sediment is discharged to the stream channel. Otherwise, all sediment is discharged to the hillslope. The portion of sediment discharged to the stream channel is a function of the particle size (see *Doten and Lettenmaier* [2004] for specific values) which is a conservative approach based on the work by *Duncan et al.* [1987]. Section 2.3 describes the particle size distribution in the roadside ditch network.

2.3. Channel Routing

[26] Sediment enters the stream and roadside ditch network as the result of debris flows originating from mass wasting or as lateral inflow from hillslopes or forest roads. All debris flows entering the channel have a fixed lognormally distributed grain size distribution [*Sturm*, 2001]. The d_{50} and d_{90} size particles of the distribution are user specified as is the number of sediment size classes, which are tracked independently. The sediment is distributed into the defined number of sediment classes according to the lognormal distribution, with the representative diameter for each class set at the median particle size for that class. Sediment from the hillslope and the road surfaces is added to the appropriate classes based on their user-specified d_{50} . The debris inflow is computed on a volumetric basis, which is converted to a mass using the *Komura* [1961] relationship for porosity of a sediment mixture, which is then converted to density:

$$P = 0.245 + 0.14d_{50}^{-0.21} \quad (5)$$

where P is porosity expressed as a fraction, and d_{50} is the median grain size in mm. The equation was developed using d_{50} over a wide range, varying from 4×10^{-4} to 80 mm.

[27] DHSVM computes channel discharge for each channel segment using a linear reservoir routing scheme. It incorporates lateral inflow via both overland flow and intercepted subsurface flow [*Wigmosta et al.*, 1994; *Wigmosta and Perkins*, 2001]. Sediment inflow to each channel segment at each time step consists of the sediment entering from the upstream reach(es), and the sediment added to the stream reach locally. Local contributions of sediment to a stream reach are uniformly distributed along the reach.

[28] The channel sediment routing is based on the work of *Wicks and Bathurst* [1996], beginning with a mass balance (similar to their equation 12). When written in terms of mass this produces the Exner equation [*Exner*, 1925].

[29] Where changes in the suspended sediment storage are small compared to the changes in bed material storage,

the channel transport equation for total load (suspended plus bed load) is:

$$\frac{\partial}{\partial t} m_s + \frac{\partial}{\partial x} ACV \rho_s = \rho_s q_s \quad (6)$$

where m_s is the mass of sediment stored in the bed per meter of channel length (kg/m); ρ_s is the sediment particle density (kg/m³); A is the cross-sectional flow area (m²), C is the total sediment concentration (m³/m³), V is the average channel flow velocity (m/s); and q_s is the local volumetric sediment inflow rate to the reach per meter of channel length (m³/s/m). Similar to the surface erosion component, the model dynamically calculates the solution time step according to the Courant condition, by setting $V\Delta t/\Delta x$ to approximately one, where Δx is the channel segment length, to maintain solution stability while minimizing run time. Because the DHSVM channel hydraulic calculations precede the sediment routing, the instantaneous upstream and downstream flow rates at each sub-time step are estimated based on the inflow and outflow rates of change. Total sediment transport capacity, in immersed weight per meter of channel width, for both the upstream and downstream flow rates is calculated using Bagnold's equation [*Bagnold*, 1966; *Graf*, 1971], which predicts total sediment transport capacity, including both suspended and bed load. The calculated transport capacity is limited to $d > 0.015$ mm [*Graf*, 1971]. Particles less than this size are considered part of the wash load and are always transportable.

[30] Changes in bed material storage, m_s , are estimated using the finite difference equation from *Wicks and Bathurst* [1996]:

$$\frac{\partial}{\partial t} m_s \approx \varphi(Q_s W_c)_i + (1 - \varphi)(Q_s W_c)_{i-1} \quad (7)$$

where i indicates the downstream end of a reach and $i-1$ the upstream end, φ is a space weighting factor (initially set to 0.55), W_c is the channel width, m, and

$$Q_s = \frac{TC_c}{g \left(1 - \frac{\rho}{\rho_s}\right)} \quad (8)$$

is the transport capacity in dry mass per unit width, kg/m/s, where TC_c is the total sediment transport capacity in immersed weight per unit channel width from Bagnold's equation, g is gravitational acceleration, and ρ is the density of water. If m_s exceeds the available sediment on the bed, it is reduced to the available sediment divided by the sub-time step length. Equation (8) is substituted into the Exner equation, which is solved for downstream sediment outflow rate for the channel reach for the current time step, t , by using the four-point finite difference formulation of *Wicks and Bathurst* [1996] which results in the sediment routing equation used in the model:

$$(ACV \rho_s)_i' = \frac{1}{\theta} \left[\theta (ACV \rho_s)_{i-1}' - (1 - \theta) \left((ACV \rho_s)_i'^{-1} - (ACV \rho_s)_{i-1}'^{-1} \right) + \rho_s q_s \Delta x - \frac{\partial}{\partial t} m_s \right] \quad (9)$$

where θ is a time-weighting factor set to 0.55 and all other terms are as previously defined. The left side of this equation is thus the sediment outflow rate in kg/s for the reach between sections i and $i-1$.

[31] Routing is performed for each particle size class starting with the smallest class. As transport capacity is used, it is not available for the remaining particle sizes. The mass of outflow for the current sub-time step accumulates for each sub-time step, up to the DHSVM time step.

3. Implementation and Testing

[32] The model was tested in the Rainy Creek tributary of the Little Wenatchee River basin, which drains the eastern slopes of the Cascade Mountains (Figure 2) in north central Washington State. It has a drainage area of approximately 44 km² and eventually discharges to the Columbia River via the Wenatchee River. It is a snowmelt-dominated catchment with mean annual precipitation ranging from 230 cm at higher elevations to 150 cm in the lower elevations according to parameter-elevation regressions on independent slope model (PRISM) maps of annual mean precipitation [Daly *et al.*, 1994, 1997].

[33] Because the sediment model was developed to predict effects of alternative land management scenarios and forest disturbance, we evaluated its performance for prediction of the effects of forest roads and fire on sediment generation in the Rainy Creek basin. We tested scenarios including the existing road network, a partially decommissioned network, and no roads, all with current (2001) vegetation data. A scenario with a simplistic representation of a catchment-wide fire was also tested.

3.1. Spatial Characteristics Data

[34] Spatial characteristics are parameters that vary grid cell by grid cell but do not change over the simulation period. They include parameters related to topography (elevation, slope, aspect) and a number of soil and vegetation characteristics. These data were provided by the U.S. Forest Service (USFS) Pacific Northwest Research Station (PNRS) and Wenatchee Forestry Sciences Laboratory (WFSL). The basin is represented by 49,085 grid cells at 30 m spatial resolution. The DEM was preprocessed in a manner similar to that of *Tarboton et al.* [1991] to fill sinks in four directions and to force flat areas to have a drainage direction. According to the DEM, the basin ranges in elevation from 630 m to 2150 m. Slopes range from 0 to 66 degrees with a mean of 26 degrees.

[35] Eight soil types are present in the basin, but over 80% of the basin is sandy or fine sandy loam (Figure 3). The soil depth map provided by the PNRS and WFSL included some soil depths in excess of 9 m, which are unrealistic for the thin-soiled Cascade mountains. On the basis of past analysis showing that slope failures in the Pacific Northwest typically occur below the root zone at depths from 0.2 to 2 m [Schmidt *et al.*, 2001], we truncated the soil depths at 2 m to be representative of rooting depths (Figure 3). Vegetation in the basin consists largely of conifers such as ponderosa pine, Douglas fir, and subalpine fir. Twenty-one vegetation classes were defined with many of the vegetation types differing only by fractional cover over the grid cell and overstory height (Figure 3).

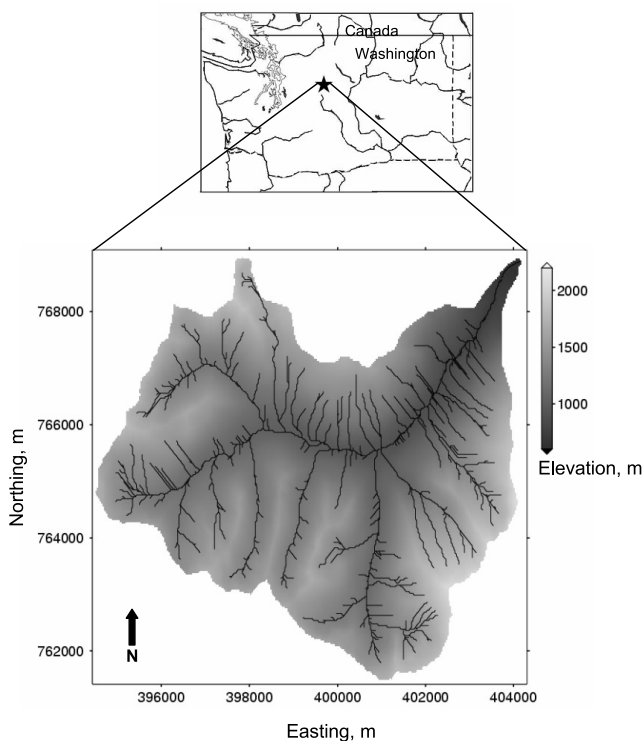


Figure 2. Rainy Creek basin site map.

[36] Total road length in the basin is 46 km and the road density is 1.05 km/km². The road network was divided at low points as well as divide locations, using the method of *Wigmosta and Perkins* [2001], resulting in 332 road segments. All road and stream intersections (91) were assumed to have culverts as were low points in the road network (193) as determined by overlaying the road network on the DEM. The extent to which the road side ditch elevations differ from the DEM elevations will determine whether each of these segments actually drains to a culvert or water bar. The most likely ramification of these assumptions is a slight overrepresentation of the culvert frequency and a conservative estimate of the effect of roads on watershed hydrology and sediment transport. Stream and roadside ditch width, depth and Manning's roughness coefficient were assigned based on classes adopted from *Storck and Lettenmaier* [2000] or information provided by PNRS and WFSL. Table 1 provides the road characteristics. Although infiltration through the road surface occurs in the overland flow model, we set this parameter to zero to provide an upper bound on erosion of road surfaces.

3.2. Temporally Varying Data

[37] The required DHSVM model forcings (precipitation, temperature, and wind speed) were taken from the nearest 1/8 degree grid cell in the continental data set of *Maurer et al.* [2002]. The remaining required forcings (relative humidity, shortwave radiation and longwave radiation) were derived from precipitation and temperature as described by *Maurer et al.* [2002]. The model adjusted this single time series to each of the DHSVM grid cells by lapsing temperature at -0.006 C/m and precipitation at 0.0007 m/m relative to a reference elevation. The model

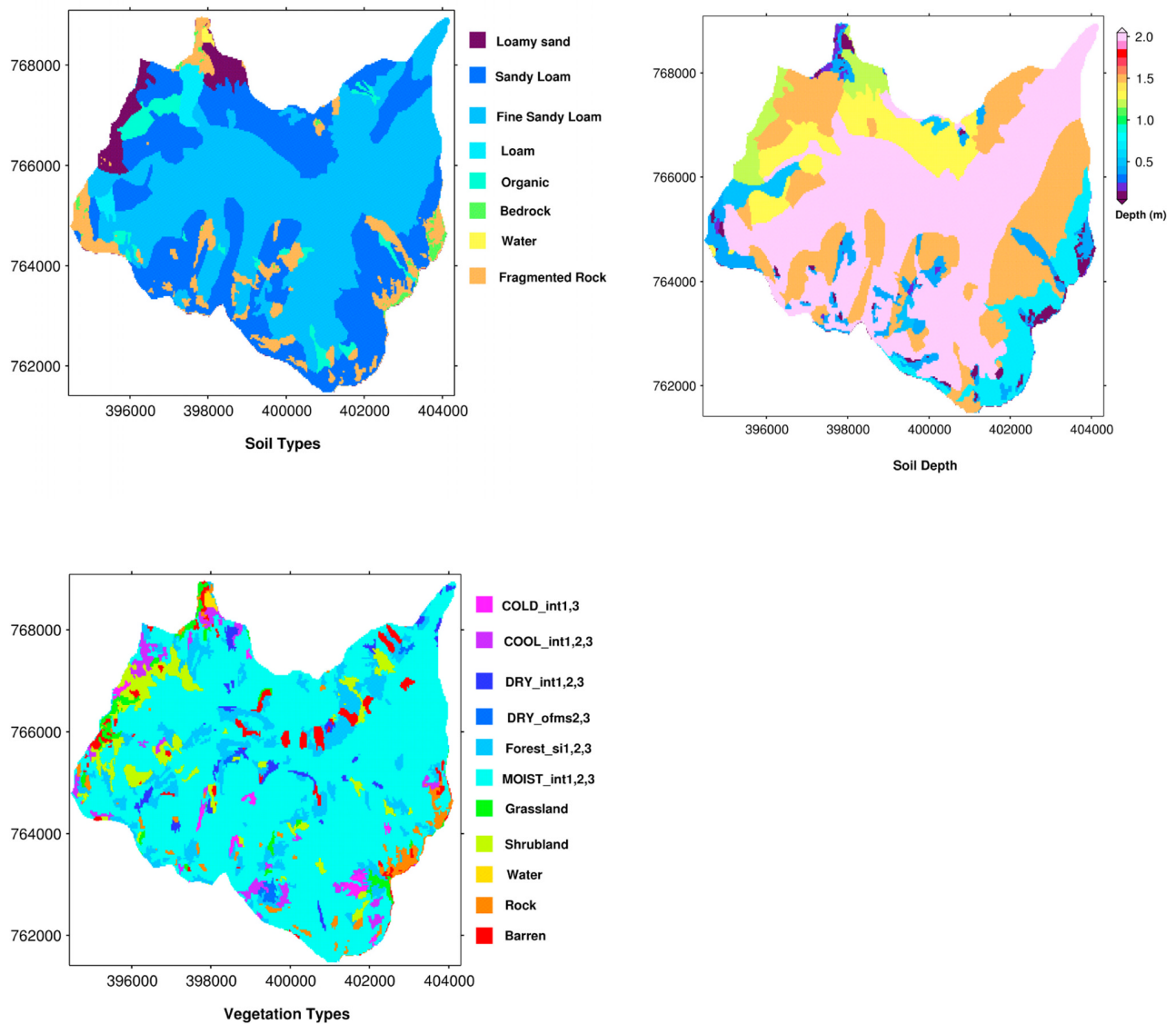


Figure 3. Rainy Creek soil and vegetation input maps.

was run at a 3 hour time step using forcing and spatial characteristics data as described above, and with other model parameters and constants taken from past model applications described by *Storck et al.* [1995], *Bowling and Lettenmaier* [2001], and *LaMarche and Lettenmaier* [2001].

3.3. Hydrology Results

[38] DHSVM was initially run from 1 October 1991 to 30 September 1995. Because Rainy Creek is ungauged, results were evaluated by comparing the predicted hydrographs to those observed for other, larger tributaries of the Wenatchee River: Chiwawa River (data from water years 1992–1997)

and Icicle Creek (data from water years 1994–1997). The simulated streamflows were compared to gauge flows scaled by basin area (Figure 4 and Table 2). According to average annual precipitation as determined using the PRISM maps [*Daly et al.*, 1994, 1997], Rainy Creek receives more precipitation than the Chiwawa River and Icicle Creek basins. Therefore the simulated hydrographs were judged to be reasonable. In addition, modeled snow water equivalent (SWE) was compared to observations at three USDA SNOTEL (snowpack telemetry) stations (Table 3 and Figure 5). These show a slight delay in modeled relative to observed snowmelt.

Table 1. Road Characteristics

Class	Description	Road Width, m	Crown Type	Ditch Width, m	Ditch Depth, m
106	road, unimproved, class 4	4.267	out-sloped	0.914	0.305
515	road, light-duty, dirt, class 3C	4.572	in-sloped	0.914	0.305
518	road, light-duty, gravel, class 3B	5.486	crowned	1.219	0.305

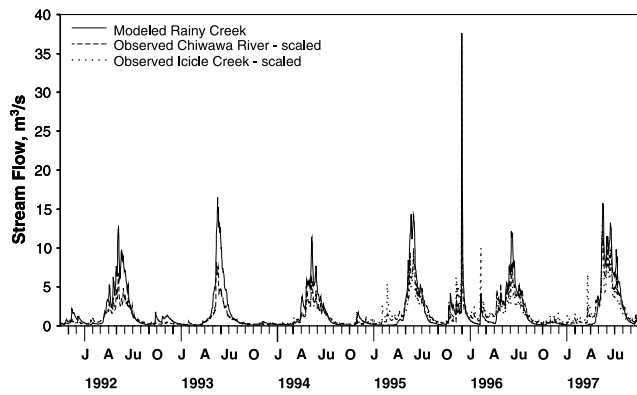


Figure 4. Modeled and observed streamflow. Observed streamflows are scaled to the Rainy Creek by basin area.

[39] Similar comparisons were made with a second DHSVM run performed for the independent period between 1 October 1995 and 30 September 1997. The streamflow hydrographs showed similar results. A large rain-on-snow event occurred in November 1995 that resulted in flood events throughout the Northern Cascades. This is shown by the decrease in SWE at the three stations accompanied by an increased flow at gauges on Chiwawa River and Icicle Creek. For Rainy Creek, no decrease in SWE or large streamflow response was initially predicted. Failure to reproduce this event indicates that the lapsed temperature based on the *Maurer et al.* [2002] data was too cold. Temperatures were subsequently adjusted to match observed air temperature trends at the three SNOTEL sites; the model then predicted the rain-on-snow event observed in the Chiwawa River and Icicle Creek hydrographs.

4. Sediment Model Implementation

[40] In addition to the input required for the DHSVM hydrology model, the sediment model requires a finer resolution DEM, additional soil and vegetation parameters, and additional road parameters. The finer resolution DEM determines the minimum width of predicted failures. Sixty-one landslides inventoried in the central California Coast Ranges had widths that clustered around 7 to 10 m [*Renau and Dietrich*, 1987], and a summary of reported shallow landslides, including the *Renau and Dietrich* [1987] inventory, showed widths of 2.7 to 40 m [*Burton et al.*, 1998]. Therefore mass wasting predictions utilized a 10 m DEM. Soil parameters required are the debris flow d_{50} (set to 2 mm) and d_{90} (set to 5 mm), particle sizes. These values represent the range of particles moved during mass wasting events. The road crown slope was set at 0.02 m/m. The required spatially variable parameters are taken from Table 1 of *Doten and Lettenmaier* [2004]. The model was run for a six year period,

from 1 October 1991 to 30 September 1997, for the existing vegetation conditions and road network. Parameters were adjusted during implementation to provide results that roughly matched published rates.

4.1. Mass Wasting

[41] Landslide rates and volumes for Rainy Creek were compiled from an aerial photograph survey [*Bergen et al.*, 2003] using five stereo pairs spanning 22 years (1970–1992). Potential slides that were in the vegetation classes “fragmented rock”, “bedrock” or “water” (as designated by the USFS vegetation map) were not included. Slides were mapped with a high, medium or low confidence level to create a series of results Slides designated as new were visible in one aerial photograph set and not in the preceding one (Table 4). All mapped slides were imported to ArcInfo and overlain on the soil depth map to estimate failed areas and volumes and failure rates. An average failure rate between 1970 and 1992 for Rainy Creek of $1.9 \text{ m}^3/\text{ha}/\text{yr}$ was determined ($3035 \text{ kg}/\text{ha}/\text{yr}$ using an average bulk density of $1600 \text{ kg}/\text{m}^3$).

[42] For the modeled time period, seven potential mass wasting events, on 8 May 1992, 18 May 1993, 30 May 1995, 29 November 1995, 08 June 1996, 17 May 1997, and 15 June 1997, were identified based on saturation screening thresholds (at least 20% of the basin had a relative saturated depth of at least 0.85). Landslide probabilities were simulated for Rainy Creek by calculating the factor of safety for 100 iterations for each of the seven events. Changes in sediment depth for each pixel over the period modeled were calculated by summing the weighted average of sediment change over all iterations for each event. Figure 6a shows the cumulative change in sediment depth, which ranged from -0.5 m (failures) to 1.3 m (runout deposition), for individual pixels for the modeled period. A simulated landslide rate of approximately $1.7 \text{ m}^3/\text{ha}/\text{yr}$ ($2882 \text{ kg}/\text{ha}/\text{yr}$), or about 95% of the rate determined from the aerial photograph survey, was determined as an average over the simulation period. Although aerial photograph mapping tends to underestimate the number of slides and landsliding rate, due to obscuring by vegetation overstory and large time gaps between photographs, another basis for comparison is the long-term erosion rate of $0.02\text{--}0.15 \text{ mm}/\text{yr}$ ($0.2\text{--}1.5 \text{ m}^3/\text{ha}/\text{yr}$) determined for the area south of Rainy Creek in the eastern Cascades by *Reiners et al.* [2003]. On the basis of elevation and inferred precipitation for Rainy Creek, the long-term erosion rate may be argued to be somewhat higher than that estimated by *Reiners et al.*, perhaps in the $0.1\text{--}0.2 \text{ mm}/\text{yr}$ ($1\text{--}2 \text{ m}^3/\text{ha}/\text{yr}$) range. In addition, rates compiled from eight Pacific Coast studies, spanning 6 to 84 years, suggest that anthropogenic influences (harvesting) may be a contributing factor in the predicted erosion rates [*Amaranthus et al.*, 1985]. They found that mass wasting rate ranged from 0.04 to $1.2 \text{ m}^3/\text{ha}/\text{yr}$ for undisturbed areas, increasing to

Table 2. Stream Gauges Utilized During DHSVM Calibration

Stream	USGS Gauge Number	Latitude	Longitude	Elevation, m	Basin Area, km^2	Average Annual Flow, m
Rainy Creek	N/A	N/A	N/A	N/A	44	N/A
Chiwawa River	12456500	$47^\circ 50' 15''$	$120^\circ 39' 40''$	640	440.3	1.15
Icicle Creek	12458000	$47^\circ 32' 38''$	$120^\circ 43' 08''$	442	499.7	1.06

Table 3. SNOTEL Stations Utilized During DHSVM Calibration

Station	Station Number	Latitude	Longitude	Elevation, m	Average Annual Precipitation, m
Fish Lake	21b04s	47°31′	121°4′	1027	1.71
Pope Ridge	20b24s	47°59′	120°34′	1078	0.92
Stevens Pass	21b01s	47°44′	121°5′	1240	2.50

0.5–3.1 m³/ha/yr and 2.9–101 m³/ha/yr for harvested and roaded areas, respectively. In any event, the simulated rate appears to be comparable to other observed landsliding rates in the region.

[43] The maximum single event probability of failure ranged from 0 to 30%. Areas that had a simulated probability of failure greater than zero for at least one event had the following characteristics: 63% had soil depth greater than 1.5 m, with 98% greater than 1 m (approximately 2% of areas with soil depth greater than both 1.5 m and 1 m, respectively), 36% had soil type of loam or organic (modeled with the same parameter distributions as loam) (16% of areas with these soil types). The remaining failed areas had soil types of either sandy loam or loamy sand. The mean slope of areas that failed was 32.1 degrees. Finally, 61% of failed areas had vegetation types with little root cohesion, including shrubland and grassland, while another 29% were barren areas with no vegetation (19% of areas with these three land cover types). Approximately 4% of the observed slides occurred in barren areas. The barren side slope areas are observed natural features of overhanging soil caused by incision along the main stem of the river. The high proportion of simulated failures in this region may indicate an underestimation of the effective cohesion for such unique features.

[44] The mapped slide locations (including slides in all confidence levels) and simulated failure areas do not always correlate well (Figure 6), due to a variety of factors. Approximately 25% of the observed slide locations coincided with a positive simulated probability of failure. Of the remaining observed slides, 30% are associated with the road corridor. While DHSVM models the effects of roads on subsurface flow, it does not represent changes in overburden or slope from road construction. The steeper cut and fill slopes not represented by the digital elevation model decrease resistance to slope failure in these locations, and are a potential initiation point for a number of the failures.

[45] Another 7% of the unpredicted observed slides occurred in the barren vegetation type where many failures were simulated. The remaining 63% of observed slides appear to have occurred in topographic hollows, where deeper soils and subsurface flow accumulate and root cohesion may not provide enough stability during large storms [Reneau and Dietrich, 1987]. The mismatch in spatial location between predicted and observed slides in both these areas is most likely due to uncertainties in spatial input data and the relative coarseness of the soil depth map.

[46] The observed slides were mapped over a 22 year period that included harvesting activities in the 1970s and 1980s. Comparison of mapped slides to a time series of peaks over threshold, with a threshold value of ~0.4 cubic meters per second based on a gauge for the Wenatchee River at Peshastin, showed that higher flows in the 1970s did not correlate with higher slide rates. This suggests that

anthropogenic influences may have been more substantial than meteorological during this period. Because our model runs utilize a temporally constant vegetation map based on April 2000 conditions that likely differs from the historic vegetation coverage, the landslide locations may understandably differ. On the basis of the information provided by USFS, the modeled vegetation can be divided into three categories loosely related to age: no overstory/stand initiation, intermediate and old growth forest. About 57% of the unpredicted mapped slides occurred in the intermediate vegetation category (Figure 6b). The majority of simulated failures (87%), occurred in the youngest vegetation category. This suggests that simulated and actual failures are more likely in younger vegetation and suggests that mismatches in failure locations are also due, at least in part, to differences in simulated and historic vegetation coverage.

4.2. Surface Erosion

[47] In an effort to reduce computation time, the hillslope erosion component was run for nine segments of the period of record when runoff was highest. During model runs, the formula for the particle detachment efficiency, β_{de} , was adjusted until the formulation specified in section 2.2.1 produced reasonable sediment detachment throughout the range of soil cohesion values. Since the specified times are likely to contribute the most erosion, they were used to determine a simulated annual rate of 1380 kg/ha. Published rates for smaller basins (McCree Creek, Burns Creek and Fox Creek) in north central Washington indicate natural surface erosion rates of 8–100 kg/ha/yr [Helvey, 1980]. These rates were determined from weir ponds and therefore are not directly comparable to the simulated results for total surface erosion which include sediment that is not deposited in the channel network. Therefore it is expected that the simulated result should be greater than the published rate. In

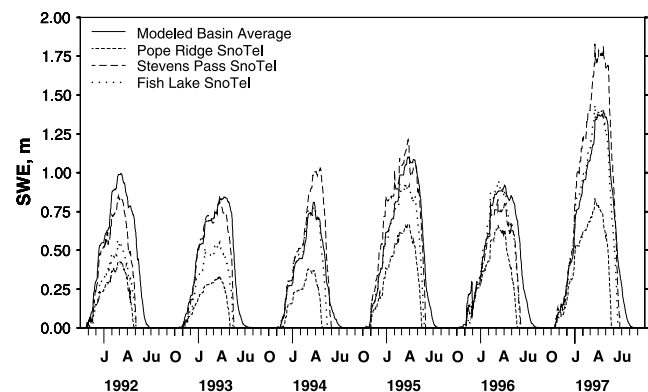


Figure 5. Modeled and observed snow water equivalent. Fish Lake SNOTEL is at elevation 1027 m, Pope Ridge is at 1078 m, and Stevens Pass is at 1240 m. The mean basin elevation is 1350 m.

Table 4. New Slides Determined From Aerial Photograph Survey

Confidence Level	1970–1975	1975–1979	1979–1986	1986–1992	Area, m ² /yr	Volume, m ³ /yr	Rate, kg/ha/yr
High	1	2	0	2	579	817	296
Medium	0	3	2	5	3017	4242	1535
Low	2	6	1	6	2629	3328	1204
Total	3	11	3	13	6225	8386	3035

addition, Rainy Creek receives more precipitation than the reference basins (58 cm at elevation 920 m) which supports the larger simulated rate.

[48] The road erosion component was run for the entire simulation period. It was run with the minimum and maximum erodibility coefficients for raindrop detachment and overland flow, described by *Smith et al.* [1999]. Initial runs with critical stream power set at the same value as in the hillslope erosion algorithm resulted in rates an order of magnitude lower than reported rates in the literature (summarized in Table 7 of *Doten and Lettenmaier* [2004]). Modifying the stream power threshold, as asserted in section 2.2.2, increased the range of annual erosion rates to 35–43 kg/ha basin area (3321–4080 kg/km of road) which is more comparable to reported values. Studies performed by *Cederholm et al.* [1981] and *Reid and Dunne* [1984] in the Clearwater Basin on the Olympic Peninsula in Washington for gravel roads with various levels of use, resulted in annual road erosion rates of 3800 to 500,000 kg/km of road (or 8,400 to 1.11×10^6 kg/ha of road, using the mean road width of 4.5 m). This basin receives significantly more precipitation (350 cm/yr) than Rainy Creek, which could explain the difference. A study by *Ketcheson et al.* [1999] in the Silver Creek area in central Idaho, showed rates of 12,000 to 55,000 kg/ha of road (5400–6750 kg/km using the same mean road width as above), 2–4 years after construction. In this case the difference cannot be explained by differences in precipitation since the basin receives less precipitation (90 cm/yr). The difference could be that our model does not account for erosion of the total road prism area including road cut and fill. In addition, materials used to construct forest roads in Idaho break down much more easily than those typically used in the Cascade Mountains.

4.3. Channel Routing

[49] The simulated sediment concentration in Rainy Creek outflow ranged from 0.01 to 179 parts per million (ppm) with a mean value of 56 ppm (Figure 7). This range seems reasonable when compared to observed concentrations in other Washington rivers (summarized in Table 7 of *Doten and Lettenmaier* [2004]). The calculated sediment yield for the modeled time period is about 830 kg/ha/yr, which again is within the range of reported values [see *Doten and Lettenmaier*, 2004, Table 8]. The algorithm initializes the sediment bed depth in each channel segment. In the beginning of the model run, much of this sediment is transported out of the network. The sediment yield during this spin-up period is not included in the results reported above.

5. Effect of Land Management Changes

[50] For all scenarios, the mass-wasting algorithm was run for the seven events specified in section 5.1. The surface erosion algorithm was run for time periods specified in

section 5.2 and the road erosion algorithm was run for the entire simulation period.

5.1. Road Scenarios

[51] The model was run for two road scenarios to evaluate the differences in (1) simulated failure probability (location and magnitude) resulting from road location on the hillslope and (2) road surface erosion for varying road density. The scenarios were a partially decommissioned network and no road (fully decommissioned) network, and they were compared to the initial run with the existing road network. USFS created the partially decommissioned road scenario by removing road segments susceptible to erosion. The summary statistics of the initial run and these scenarios are provided in Table 5. Relative to past assessments of the effects of forest roads on basin hydrology using

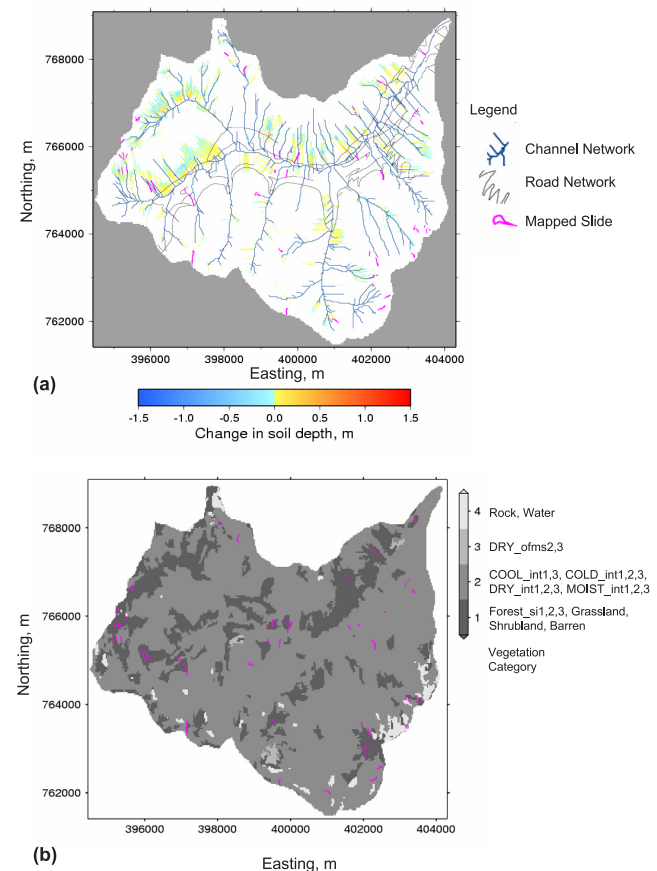


Figure 6. (a) Change in soil depth overlay with aerial photograph mapped landslides. Blue areas represent failures, while yellow/orange areas represent deposition. White area indicates no change in soil depth. (b) Year 2000 vegetation categories overlay with aerial photograph mapped landslides.

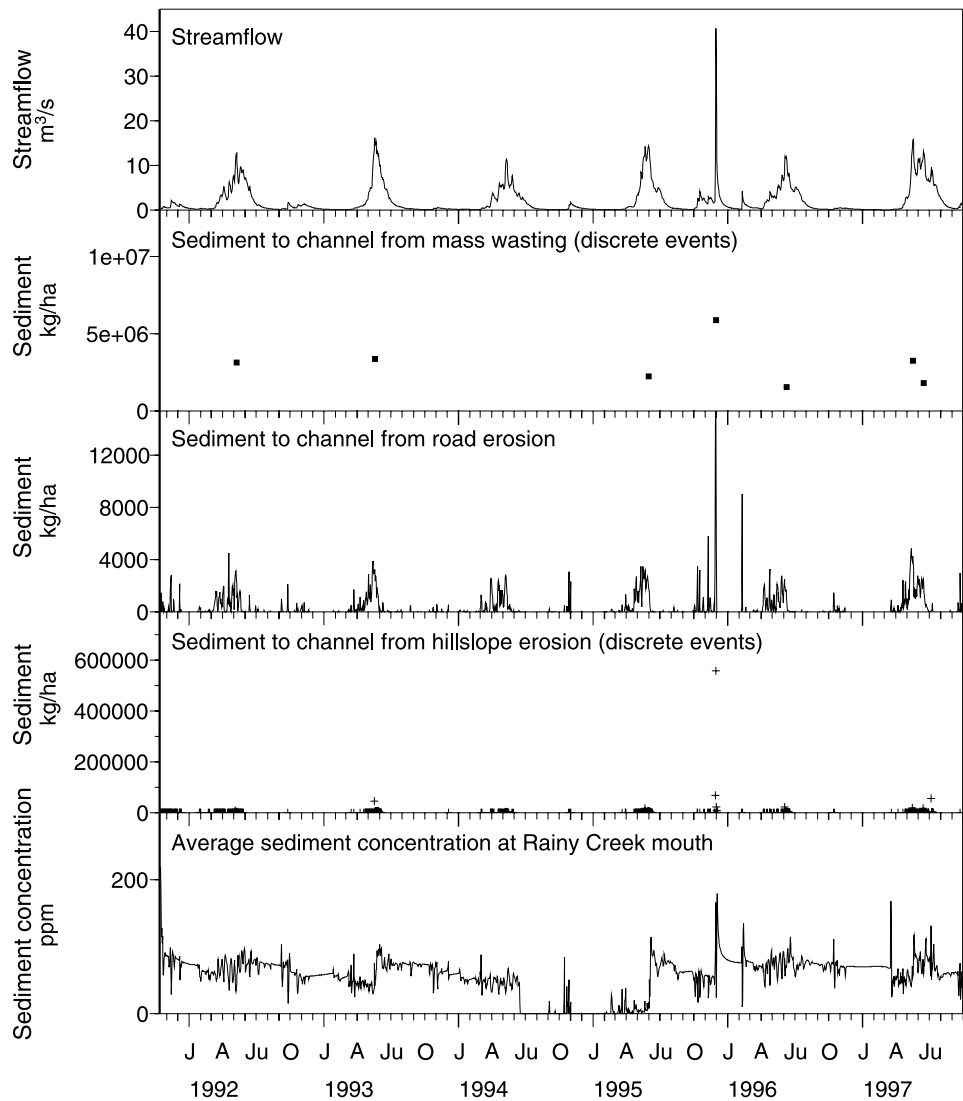


Figure 7. Modeled streamflow, sediment inputs to the channel network, and sediment concentration at Rainy Creek outflow. The mass-wasting algorithm was run on 8 May 1992, 18 May 1993, 30 May 1995, 29 November 1995, 8 June 1996, 17 May 1997, and 15 June 1997. The hillslope erosion algorithm was run during periods for high modeled runoff: 5–12 May 1992, 18–31 May 1993, 8–15 May 1994, 21 May to 6 June 1995, 28 November to 3 December 1995, 4–18 June 1996, 16–May 1997, 14–20 June 1997, and 6–12 July 1997. Peaks in sediment concentration occur with peaks in streamflow and sediment inputs from mass wasting.

DHSVM, the road density of 1.05 km/km^2 in Rainy Creek is small. In particular, *LaMarche and Lettenmaier* [1998] and *Bowling and Lettenmaier* [2001] used DHSVM to model the Deschutes River subbasins, which had road densities that varied from 3.2 to 5.0 km/km^2 . Their simulations showed an increase in peak flows and an average

change in peaks over threshold from 1.8 to 9.0% . While the effect of roads on basin hydrology is the result of a number of road characteristics, the larger the road network the greater the potential for changes in hydrology. The relatively small change in the road network for the road scenarios in Rainy Creek showed less than a 1% change in annual peak

Table 5. Road Scenarios

Road Network	Road Density, km/km^2	Number of Culverts	Total Road Surface Area, km^2	Percent Area by Class		
				106	515	518
Existing	1.05	284	0.23	10.36	40.00	49.64
Partially decommissioned	0.75	202	0.17	<1	30.53	69.45
None	0	0	0	0	0	0

Table 6. Road Scenario Results: Basin Average Annual Rates

Road Network	Sediment Yield, kg/ha	Landslide Rate, ^a kg/ha	Hillslope Erosion Rate, ^b kg/ha	Road Erosion Rate, kg/ha	Road Erosion Rate, kg/km of road
Existing	830	2882	1380	35–43 (6,717–8,205) ^c	3321–4080
Partially decommissioned	780	2849	1380	5–6 (1,266–1,609) ^c	671–806
None	800	2851	1386	0	0

^aThe mass-wasting algorithm was run on 8 May 1992, 18 May 1993, 30 May 1995, 29 November 1995, 8 June 1996, 17 May 1997, and 15 June 1997.

^bThe hillslope erosion algorithm was run during periods for high modeled runoff: 5–12 May 1992, 18–31 May 1993, 8–15 May 1994, 21 May to 6 June 1995, 4–18 June 1996, 16–21 May 1997, 14–20 June 1997, and 6–12 July 1997. Since these times are likely to contribute the most erosion, they were used to determine the annual rate.

^cValue in parenthesis is road erosion rate per hectare of road area.

flows. There were minor changes (average from 0.02 to 0.03) in simulated saturated fraction (saturated depth/soil depth) for the mass-wasting events.

[52] In order to isolate the effects of forest roads on simulated basin hydrology and thus probability of failure, the scenarios were run with the same random number sequences as the initial run. This means that while parameters varied spatially and temporally throughout the basin, all scenarios had the same values within each pixel at the same time.

[53] The results of the road scenario analyses are summarized in Table 6. Simulated basin average road erosion decreased with decreasing road area as expected. Road erosion rates per unit road area increased with road area, because not all road segments have enough surface runoff to cause erosion and partial decommissioning was intended to remove segments with high erosion rates. Hillslope erosion increased with decreasing road area, due to longer flow paths.

[54] Figures 8a and 8b show the difference (existing - scenario) in the change in maximum failure probability for

the partially decommissioned and fully decommissioned road scenarios, respectively. While the computed failure rates are similar for the two scenarios, the spatial distribution of changes in soil depth and failure probability differs, due to the effects of the road network on basin hydrology. Prior empirical studies typically report an increase in mass wasting with increasing road density, but the model does not represent some aspects of road/hydrology interaction, such as culvert blockage, and/or overtopping that can lead to the failure of roads themselves, including cut and fill slopes, and these mechanisms, if represented, would likely result in larger predicted changes. The modest changes simulated may also be attributable to the relatively small current road density: the changes in soil moisture are not large enough to result in substantial differences in slope failure rates.

[55] As previously mentioned, the magnitude of the effect of roads on basin hydrology is a function of a number of characteristics, i.e., location in the hillslope and upslope contributing area, depth of roadside ditches, culvert spacing and road drainage connectivity to the stream network. These

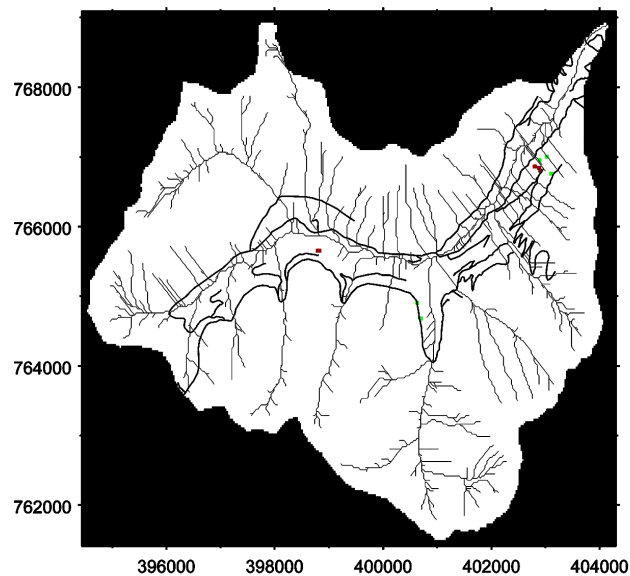


Figure 8a. Difference in maximum event probability of failure between partially decommissioned road network and existing road network. Red indicates model pixels for which probability of failure was reduced by more than 0.005; green indicates pixels for which failure probability was increased by more than 0.005.

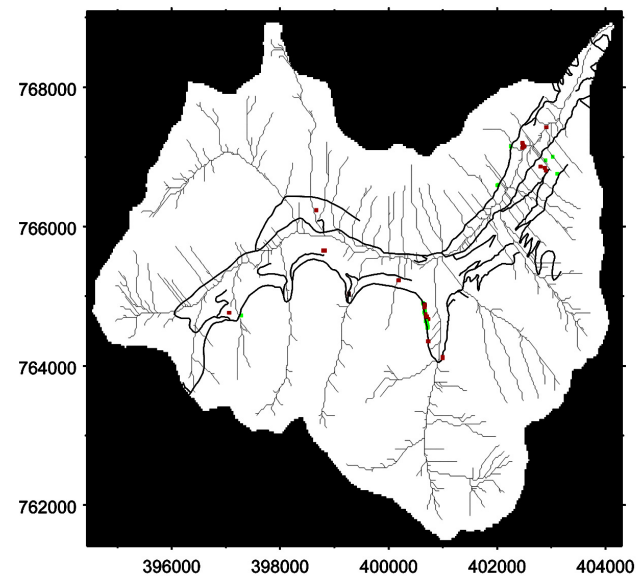


Figure 8b. Difference in maximum event probability of failure between completely decommissioned road network and existing road network. Red indicates model pixels for which probability of failure was reduced by more than 0.005; green indicates pixels for which failure probability was increased by more than 0.005.

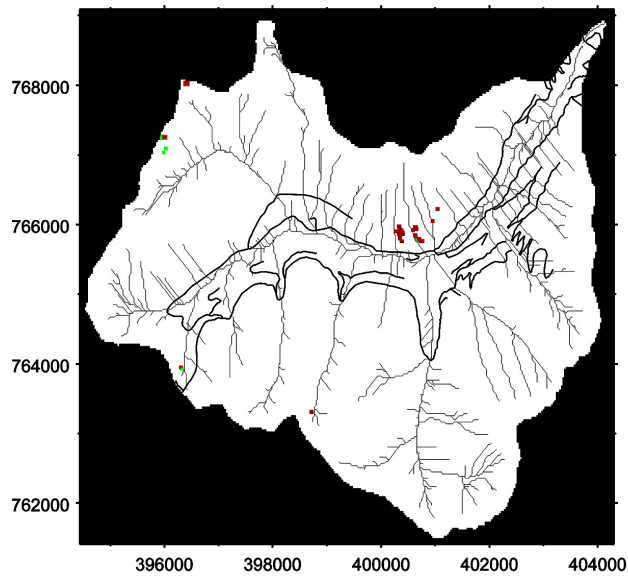


Figure 9. Difference in maximum event probability of failure associated with fire scenario relative to current conditions. Red indicates model pixels for which probability of failure increased by more than 0.005; green indicates pixels for which failure probability decreased by more than 0.005.

effects on basin hydrology, in turn, affect the probability of failure by causing changes in soil moisture. The density of culverts, either due to increased road density or road construction methods, and the culvert discharge location will determine the magnitude and location of these effects (it should be noted that the culvert locations were specified based on the assumptions stated in section 4.1; culvert locations were not field verified). Roads concentrate flow prior to discharging it to the hillslope or the stream network. Therefore, if the discharge location is more stable and the intercepted water is from an unstable area, the simulated result will be a decrease in failure probability.

5.2. Fire Scenario

[56] The model was run (with the existing road network) for a fire scenario to evaluate changes in erosion rates due to the effects of (1) changes in soil moisture, surface runoff and streamflow due to reduced leaf area index (LAI) and loss of understory and (2) reduction in root cohesion. Fire effects were simulated by removing the understory from all pixels with an overstory, setting the LAI of pixels with an overstory to 1.0, and reducing the root cohesion

distributions of the pixels with an overstory by 2 kPa, simulating the loss of understory. Woody shrubs and ground-cover typically have root cohesion < 3 kPa [Montgomery *et al.*, 1998]. These modifications were held constant throughout the 6 year simulation.

[57] Figure 9 shows differences in maximum failure probability between existing conditions and postfire conditions. The results are summarized in Table 7. The fire scenario results in decreased evapotranspiration due to reduced LAI. Total simulated streamflow increased by 9%, surface runoff increased by 13%, but the average saturated area in the basin increased by only 0.14%. The mass-wasting rate increased by 11% due to the decreased root cohesion. The hillslope erosion rate increased due to more particle detachment from additional raindrop and leaf drip energy due to the removal of the understory, and increased runoff and thus transport capacity. In the model, the fractional coverage of the overstory is used to modify the precipitation throughfall over the entire pixel. The model does not explicitly represent the location of overstory within a pixel. Because of decreased LAI of the overstory and loss of the understory, less precipitation was intercepted by the overstory resulting in more precipitation reaching the road surface. This results in higher road runoff, because there is no infiltration on the road surface. The road erosion rate increased due to the additional runoff and transport capacity.

[58] Sediment yield increased approximately in proportion to the additional inputs to the channel network. In all scenarios, all but the largest particles from debris flows were transported out of the basin. Colluvium may accumulate in low-order channel segments between episodes of debris flow scour [e.g., Benda, 1990]. Modeled sediment transport showed that storms causing large sediment inputs would not typically transport all the material, but streamflow between events and the following snowmelt runoff tended to remove the material from the channel.

6. Conclusions

[59] We have presented an approach to predicting erosion and sediment transport using the DHSVM framework. The approach includes the main sources of sediment supply in forested mountainous watersheds: mass wasting, hillslope erosion, and forest road erosion. It includes sediment routing from these sources to the stream channel network as well as routing through the network. A test application to the Rainy Creek catchment shows that the model produces plausible sediment yields in comparison with literature values for similar catchments. Likewise, ratios of landsliding and surface erosion rates are plausible when compared

Table 7. Fire Scenario Results: Basin Average Annual Rates

Scenario	Sediment Yield, kg/ha	Landslide Rate, ^a kg/ha	Hillslope Erosion Rate, ^b kg/ha	Road Erosion Rate, kg/ha	Road Erosion Rate, kg/km of road
Existing	830	2882	1380	34 (6,452) ^c	3226
Fire	850	3205	2099	37 (7,154) ^c	3510

^aThe mass-wasting algorithm was run on 8 May 1992, 18 May 1993, 30 May 1995, 29 November 1995, 8 June 1996, 17 May 1997, and 15 June 1997.

^bThe hillslope erosion algorithm was run during periods for high modeled runoff: 5–12 May 1992, 18–31 May 1993, 8–15 May 1994, 21 May to 6 June 1995, 4–18 June 1996, 16–21 May 1997, 14–20 June 1997, and 6–12 July 1997. Since these times are likely to contribute the most erosion, they were used to determine the annual rate.

^cValue in parenthesis is road erosion rate per hectare of road area.

to published rates for various watersheds in the Pacific Northwest.

[60] The model was applied to compare the effects of reducing road densities on erosion and sediment transport in the Rainy Creek drainage. This scenario showed only small changes in mass-wasting rates and sediment yield, and some spatial changes in mass-wasting locations. Also, as road density decreased the road erosion rate/road area decreased. Larger changes were not realized, either due to the limited hydrologic changes caused by the roads, the construction of roads at low elevation along the main channel, or because road characteristics that contribute to road-related mass wasting (i.e., blocked culverts) are not represented in the model. A second scenario, representing a forest fire, showed an increase in all erosion components due to decreases in root cohesion and increases in surface runoff and thus transport capacity.

[61] **Acknowledgments.** Financial support for the work reported herein was provided by the USFS Pacific Northwest Research Station and Wenatchee Forestry Sciences Laboratory under Research Joint Venture agreement 00-RJVA-11261927-522. Thanks are owed to Kristian Bergen (Harvard University) for his assistance with the aerial photograph landslide survey and to Ted Bohn (University of Washington) for his assistance with development of the computer code.

References

- Amaranthus, M. P., R. M. Rice, N. R. Barr, and R. R. Ziemer (1985), Logging and forest roads related to increased debris slides in southwestern Oregon, *J. For.*, *83*, 229–233.
- Ascough, J. C., II, C. Baffaut, M. A. Nearing, and B. Y. Liu (1997), The WEPP watershed model: I. Hydrology and erosion, *Trans. ASAE*, *40*, 921–933.
- Bagnold, R. A. (1966), An approach of sediment transport model from general physics, *U.S. Geol. Surv. Prof. Pap.*, 422-J.
- Benda, L. (1990), The influence of debris flows on channels and valley floors of the Oregon Coast Range, U.S.A., *Earth Surf. Processes Landforms*, *15*, 457–466.
- Benda, L., and T. Dunne (1997), Stochastic forcing of sediment supply to channel networks from landsliding and debris flow, *Water Resour. Res.*, *33*, 2849–2863.
- Bergen, K. J., C. O. Doten, and D. P. Lettenmaier (2003), Landslide rates in the Eastern Cascade Mountain Range, *Eos Trans. American Geophysical Union*, *84*(46), Fall Meet. Suppl., Abstract H51D–1097.
- Beven, K. J., and M. J. Kirkby (1979), A physically based, variable contributing area model of basin hydrology, *Hydrol. Sci. Bull.*, *24*, 43–69.
- Bowling, L. C., and D. P. Lettenmaier (2001), The effects of forest roads and harvest on catchment hydrology in a mountainous maritime environment, in *Land Use and Watersheds: Human Influence on Hydrology and Geomorphology in Urban and Forest Areas*, *Water Sci. Appl. Ser.*, vol. 2, edited by M. S. Wigmosta and S. J. Burges, pp. 145–164, AGU, Washington, D. C.
- Burton, A., and J. C. Bathurst (1998), Physically based modeling of shallow landslide sediment yield at a catchment scale, *Environ. Geol.*, *35*, 89–99.
- Burton, A., T. J. Arkell, and J. C. Bathurst (1998), Field variability of landslide model parameters, *Environ. Geol.*, *35*, 110–115.
- Cederholm, C. J., L. M. Reid, and E. O. Salo (1981), Cumulative effects of logging road sediment on salmonid populations in the Clearwater River, Jefferson County, Washington, in *Proceedings, Conference on Salmon-Spawning Gravel: A Renewable Resource in the Pacific Northwest?*, *Water Res. Cent. Rep.* 39, pp. 38–74, Wash. State Univ., Pullman.
- Chow, V. T., D. R. Maidment, and L. W. Mays (1988), *Applied Hydrology*, 572 pp., McGraw-Hill, New York.
- Daly, C., R. P. Neilson, and D. L. Phillips (1994), A statistical-topographic model for mapping climatological precipitation over mountainous terrain, *J. Appl. Meteorol.*, *33*, 140–158.
- Daly, C., G. H. Taylor, and W. P. Gibson (1997), The PRISM approach to mapping precipitation and temperature, paper presented at 10th Conference on Applied Climatology, Am. Meteorol. Soc., Reno, Nev.
- Dhakal, A. S., and R. C. Sidle (2003), Long-term modelling of landslides for difference forest management practices, *Earth Surf. Process. Landforms*, *28*, 853–868.
- D’Odorico, P., S. Fagherazzi, and R. Rigon (2005), Potential for landsliding: Dependence on hyetograph characteristics, *J. Geophys. Res.*, *110*, F01007, doi:10.1029/2004JF000127.
- Doten, C. O., and D. P. Lettenmaier (2004), Prediction of sediment erosion and transport with the distributed hydrology-soil-vegetation model, *Water Resour. Ser. Tech. Rep.* 178, Dep. of Civ. and Environ. Eng., Univ. of Wash., Seattle. (Available at <http://www.hydro.washington.edu/Lettenmaier/Publications.html#2002R>)
- Duncan, S. H., R. F. Bilby, J. W. Ward, and J. T. Heffner (1987), Transport of road-surface sediment through ephemeral stream channels, *Water Resour. Bull.*, *23*, 113–119.
- Exner, F. M. (1925), Ber die wechselwirkung zwischen wasser und geschiebe inflssen, Sitzungsber, *Akad. Wiss. Wien Math. Naturwiss. Abt. 2A*, *134*, 165–180.
- Govers, G. (1992), Evaluation of transporting capacity formulae for overland flow, in *Overland Flow: Hydraulics and Erosion Mechanics*, edited by J. A. Parsons and A. D. Abrahams, CRC Press, Boca Raton, Fla.
- Graf, W. (1971), *Hydraulics of Sediment Transport*, pp. 208–211, McGraw-Hill, New York.
- Hammond, C., D. Hall, S. Miller and P. Swetik (1992), Level I Stability Analysis (LISA), documentation for version 2.0, *Gen. Tech. Rep. INT-285*, Intermt. Res. Stn., U.S. Dep. of Agric., Ogden, Utah.
- Helvey, J. P. (1980), Effects of a north central Washington wildfire on runoff and sediment production, *Water Resour. Bull.*, *16*, 627–634.
- Ketcheson, G. L., W. F. Megahan, and J. G. King (1999), “R1-R4” and “BOISED” sediment production model tests using forest roads in granitics, *J. Am. Water Resour. Assoc.*, *35*, 83–98.
- Koler, T. E. (1998), Evaluating slope stability in forest uplands with deterministic and probabilistic models, *Environ. Eng. Geosci.*, *4*, 185–194.
- Komura, W. (1961), Bulk properties of river sediments and their application to sediment hydraulics, paper presented at 11th Japan National Congress, Japan Natl. Comm. for Theor. and Appl. Mech., Tokyo.
- LaMarche, J., and D. P. Lettenmaier (1998), *Forest road effects on flood flows in the Deschutes River Basin*, *Washington, Water Resour. Ser. Tech. Rep.* 158, Univ. of Wash., Seattle.
- LaMarche, J., and D. P. Lettenmaier (2001), Effects of forest roads on flood flows in the Deschutes Basin, Washington, *Earth Surf. Processes Landforms*, *26*, 115–134.
- Leung, L. R., and M. S. Wigmosta (1999), Potential climate change impacts on mountain watersheds in the Pacific Northwest, *J. Am. Water Resour. Assoc.*, *35*, 1463–1471.
- Maurer, E. P., A. W. Wood, J. C. Adam, D. P. Lettenmaier, and B. Nijssen (2002), A long-term hydrologically-based data set of land surface fluxes and states for the conterminous United States, *J. Clim.*, *15*, 3237–3251.
- Montgomery, D. R., K. Sullivan, and H. M. Greenberg (1998), Regional test of a model for shallow landsliding, *Hydrol. Processes*, *12*, 943–955.
- Morgan, R. P. C., J. N. Qinton, R. E. Smith, G. Govers, J. W. A. Poesen, K. Auerswald, G. Chisci, D. Torri, and M. E. Styczen (1998), The European soil erosion model (EUROSEM): A dynamic approach for predicting sediment transport from fields and small catchments, *Earth Surf. Processes Landforms*, *23*, 527–544.
- Nijssen, B., I. Haddeland, and D. P. Lettenmaier (1997), Point evaluation of a surface hydrology model for BOREAS, *J. Geophys. Res.*, *102*, 29,367–29,378.
- Reid, L. M., and T. Dunne (1984), Sediment production from forest road surfaces, *Water Resour. Res.*, *20*, 1753–1761.
- Reiners, P. W., T. A. Ehlers, S. G. Mitchell, and D. R. Montgomery (2003), Coupled spatial variation in precipitation and long-term erosion rates across the Washington Cascades, *Nature*, *426*, 645–647.
- Reneau, S. L., and W. E. Dietrich (1987), Size and location of colluvial landslides in a steep forested landscape, in *Erosion and Sedimentation in the Pacific Rim*, edited by R. L. Beschta et al., *IAHS Publ.*, *165*, 39–48.
- Schmidt, K. M., J. J. Roering, J. J. Stock, W. E. Dietrich, D. R. Montgomery, and T. Schaub (2001), Root cohesion variability and shallow landslide susceptibility in the Oregon Coast Range, *Can. Geotech. J.*, *38*, 995–1024.
- Selby, M. J. (1982), *Hillslope Materials and Processes*, Oxford Univ. Press, New York.
- Sidle, R. C., A. J. Pearce, and C. L. O’Loughlin (1985), *Hillslope Stability and Land Use*, *Water Resour. Monogr. Ser.*, vol. 11, AGU, Washington, D. C.
- Smith, R. E., and J. Y. Parlange (1978), A parameter-efficient hydrologic infiltration model, *Water Resour. Res.*, *14*, 533–538.
- Smith, R. E., D. C. Goodrich, D. A. Woolhiser, and C. L. Unkrich (1995), KINEROS—A kinematic runoff and erosion model, in *Computer Models*

- of *Watershed Hydrology*, edited by V. P. Singh, pp. 697–732, Water Resour. Publ., Highlands Ranch, Colo.
- Smith, R. E., D. C. Goodrich, and C. L. Unkrich (1999), Simulation of selected events on the Catsop catchment by KINEROS2, a report for the GCTE conference on catchment scale erosion models, *Catena*, 37, 457–475.
- Storck, P., and D. P. Lettenmaier (2000), Trees, snow and flooding: An investigation of forest canopy effects on snow accumulation and melt at the plot and watershed scales in the Pacific Northwest, *Water Resour. Ser. Tech. Rep. 161*, Dep. of Civ. and Environ. Eng., Univ. of Wash., Seattle.
- Storck, P., D. P. Lettenmaier, B. A. Connelly, and T. W. Cundy (1995), Implications of forest practices on downstream flooding, phase II, final report, Univ. of Wash., Seattle.
- Storck, P., L. Bowling, P. Wetherbee, and D. Lettenmaier (1998), Application of a GIS-based distributed hydrology model for prediction of forest harvest effects on peak stream flow in the Pacific Northwest, *Hydrol. Processes*, 12, 889–904.
- Sturm, T. (2001), *Open Channel Hydraulics*, pp. 378–380, McGraw-Hill, New York.
- Tarboton, D. G., R. L. Bras, and I. Rodriguez-Iturbe (1991), On the extraction of channel networks from digital elevation data, *Hydrol. Processes*, 5, 81–100.
- Ward, T. J., R. Li, and D. B. Simons (1981), Use of a mathematical model for estimating potential landslide sites in steep forested drainage basins, in *Erosion and Sediment Transport in Pacific Rim Steeplands*, edited by T. R. H. Davies and A. J. Pearce, *IAHS Publ.*, 132, 21–41.
- Whitaker, A. Y., Y. Alila, J. Beckers, and D. Toews (2002), Evaluating peak flow sensitivity to clear-cutting in different elevation bands of a snow-melt-dominated mountainous catchment, *Water Resour. Res.*, 38(9), 1172, doi:10.1029/2001WR000514.
- Whitaker, A. Y., Y. Alila, J. Beckers, and D. Toews (2003), Application of the distributed hydrology, soil vegetation model to redfish creek, British Columbia: Model evaluation using internal catchment data, *Hydrol. Processes*, 17, 199–224.
- Wicks, J. M., and J. C. Bathurst (1996), SHESED: A physically based, distributed erosion and sediment yield component for the SHE hydrological modeling system, *J. Hydrol.*, 175, 213–238.
- Wigmosta, M. S., and D. P. Lettenmaier (1999), A comparison of simplified methods for routing topographically-driven subsurface flow, *Water Resour. Res.*, 35, 255–264.
- Wigmosta, M. S., and W. A. Perkins (2001), Simulating the effects of forest roads on watershed hydrology, in *Land Use and Watersheds: Human Influence on Hydrology and Geomorphology in Urban and Forest Areas*, *Water Sci. Appl. Ser.*, vol. 2, edited by M. S. Wigmosta and S. J. Burgess, pp. 127–143, AGU, Washington, D. C.
- Wigmosta, M. S., L. W. Vail, and D. P. Lettenmaier (1994), A distributed hydrology-vegetation model for complex terrain, *Water Resour. Res.*, 30, 1665–1669.
- Wischmeier, W. H., and D. D. Smith (1965), Predicting rainfall-erosion losses from cropland east of the Rocky Mountains, *Rep. AH-282*, 47 pp., U.S. Dep. of Agric., Washington, D. C.
- Woolhiser, D. A., R. E. Smith, and D. C. Goodrich (1990), KINEROS, a kinematic runoff and erosion model: Documentation and user manual, *Rep. ARS-77*, 130 pp., Agric. Res. Serv., U.S. Dep. of Agric., Washington, D. C.
- Wu, W., and R. C. Sidle (1995), A distributed slope stability model for steep forested basins, *Water Resour. Res.*, 31, 1097–1110.
- Ziegler, A. D., T. W. Giambelluca, and R. A. Sutherland (2001), Erosion prediction on unpaved mountain roads in northern Thailand: Validation of dynamic erodibility modeling using KINEROS2, *Hydrol. Processes*, 15, 337–358.

L. C. Bowling, Department of Agronomy, Purdue University, Lilly Hall of Life Sciences, 915 West State Street, West Lafayette, IN 47907, USA.

C. O. Doten, J. S. Lanini, and D. P. Lettenmaier, Department of Civil and Environmental Engineering, University of Washington, Seattle, WA 98195, USA. (dennisl@u.washington.edu)

E. P. Maurer, Department of Civil Engineering, Santa Clara University, 500 El Camino Real, Santa Clara, CA 95053, USA.